

Diffuse x-ray scattering from weakly metamict zircon

This article has been downloaded from IOPscience. Please scroll down to see the full text article.

1999 J. Phys.: Condens. Matter 11 8947

(<http://iopscience.iop.org/0953-8984/11/45/317>)

[View the table of contents for this issue](#), or go to the [journal homepage](#) for more

Download details:

IP Address: 171.66.16.220

The article was downloaded on 15/05/2010 at 17:49

Please note that [terms and conditions apply](#).

Diffuse x-ray scattering from weakly metamict zircon

S Ríos[†] and E K H Salje

Department of Earth Sciences, University of Cambridge, Downing Street, Cambridge CB2 3EQ, UK

Received 14 May 1999, in final form 4 August 1999

Abstract. Diffuse x-ray (Cu K α_1) scattering from α -decay radiation-damaged natural zircon has been investigated at room temperature. Huang scattering around Bragg reflections was observed in samples with radiation doses between 0.06 and 2×10^{18} α -decay events g $^{-1}$, but none in a highly crystalline natural zircon sample ($<0.01 \times 10^{18}$ α -decay events g $^{-1}$). Huang scattering ($\sim q^{-2}$) dominates for small wavevectors, while Stokes–Wilson scattering ($\sim q^{-4}$) is observed at larger values of q from the Bragg reflection. The displacement field produced by α -decay radiation damage is shown to correspond to transverse shear waves. The unit-cell expansion observed in zircon is thus interpreted as originating as a consequence of the shear waves propagating in the crystal, rather than from simply longitudinal expansion waves. A cluster size between 70 and 140 Å, depending on the degree of damage, characterizes the defect accumulation.

1. Introduction

Natural zircon (ZrSiO₄, $I4_1/AMD$, $Z = 4$) is known to undergo a radiation-induced amorphization process as a consequence of the α -decay of radiogenic impurities, mainly U and Th (Holland and Gottfried 1955, Chakoumakos *et al* 1987, Ewing *et al* 1987). The origin of the radiation damage in zircon is twofold: while the recoil nucleus creates islands of disordered material by displacing several thousands of atoms, the α -particle itself creates, at the end of its path, several hundreds of isolated defects. Such defects are often referred to as Frenkel pairs although their atomic structure is still unknown. This amorphization process has been commonly understood in terms of a phase transition from the original crystalline state to the highly aperiodic state, the so-called metamict state. However, a new interpretation has been recently proposed where the transformation is related to the percolation of either the crystalline material in an amorphous matrix or the amorphous material in a crystalline matrix (Salje *et al* 1999). At the percolation point, the minority state (amorphous islands at low radiation doses or crystalline islands at high radiation doses) starts to form an interconnected network.

At low radiation doses in zircon ($<3 \times 10^{18}$ α -decay events g $^{-1}$, below the first percolation point (Salje *et al* 1999)) less than 20% of the total volume is aperiodic, the rest of the original crystal being mainly crystalline with only some distorted or damaged areas. At this stage, when amorphous areas are still isolated, the size of these amorphous regions was estimated from high-resolution transmission electron microscopy images to be about 50 Å (Chakoumakos *et al* 1987, Murakami *et al* 1991, Weber *et al* 1994). However, not much is known about the defects created in the crystalline part of the material by the α -particles themselves. These two distinct mechanisms of destruction of the original crystal are expected to have different effects

[†] Author to whom any correspondence should be addressed.

on the crystalline matrix of zircon. As shown in a previous work on UO_2 (Weber 1981), the swelling of the unit-cell parameter provoked by α -particles has double the importance (at the saturation dose) of the swelling produced by the α -recoil nucleus. For zircon, the only certain information so far appears to be the fact that such local defects lead to an increase of the lattice parameters.

Previous works on polycrystalline samples of damaged zircons (Ewing *et al* 1987, Murakami *et al* 1991) have investigated the diffuse scattering arising from the radiation damage process. Nevertheless, little could be derived from such studies about the physical nature of the defects because of the following limitations. First of all, powder diffraction measurements average over many grains and orientations. This makes the distinction between, e.g., strain effects and heterogeneities of the sample virtually impossible. Secondly, grinding-damaged material introduces additional defects which cannot be separated from 'intrinsic' defects.

It is known from works on noble metals (Trinkaus (1972), Dederichs (1973) and references therein) that single-crystal diffuse scattering is a powerful technique for investigating defects and their clusters. From the distribution of the diffuse intensity around the Bragg reflection of structurally simple materials (Cu, Ni, Si, ...) one may extract information about the symmetry and the strength of the defects. At present, there has been hardly any detailed study of the α -decay radiation-damage-created defects in zircon. With the purpose of getting an insight into the defective areas produced in the early stages of this process, diffuse x-ray scattering measurements were carried out on four different natural zircon samples (the radiation dose was lower than $2 \times 10^{18} \alpha$ -decay events g^{-1}). At this stage the unit-cell swelling ($\Delta V/V_0$) reaches a value of $\approx 2\%$ (Holland and Gottfried 1955, Murakami *et al* 1991). Measurements were carried out close to the Bragg reflections: typically $(h00)$, $(hh0)$ and $(h0l)$.

We report in this paper the results of the first systematic study by diffuse x-ray scattering of α -decay radiation damage in zircon. We shall argue that the radiation damage produces mainly shear deformation in the crystalline lattice, the expansion of the unit cell being only a secondary effect.

2. Experimental procedure

2.1. Samples

Single crystals of four natural zircons with different degrees of radiation damage were used for this study (table 1). Sample PHN 4100G, with a very low content of radiogenic impurities, was from the Solomon Islands (Nowell 1999). Sample 4403, from Sri Lanka, had already been characterized in a previous work (Murakami *et al* 1991). The Moroto sample was from the locality with the same name in Eastern Uganda, and sample 269 was also from Sri Lanka. The latter two samples were characterized for this study as described below. Individual crystals varied in size from ≈ 2 to 5 mm in their longest dimension. The colours were dark orange and light pink for samples 4403 and Moroto respectively, whereas samples PHN 4100G and 269 were transparent. The compositions of the Moroto and 269 samples were determined

Table 1. The α -decay-event dose of radiation-damaged zircon samples.

Sample	U/Th (ppm)	Dose ($10^{18} \alpha$ -decay events g^{-1})
PHN 4100G	5/—	< 0.01
4403	$26 \pm 4/31 \pm 5$	0.06
Moroto	$425 \pm 70/—$	1.1
269	$1090 \pm 100/—$	1.8

by using an electron microprobe CAMECA SX50 operated in the energy-dispersive mode at an accelerating voltage of 20 kV with a beam diameter of 1 μm . The detection limits for U and Th elements were improved by using a sample current of 150 mA with a counting time of up to 20 min. The minimum detection limits for U and Th elements were about 200 ppm (by weight). The Th concentrations in the Moroto and 269 samples were below our detection limits.

2.2. X-ray diffraction

Each of the samples described above was first oriented, and subsequently analysed using a seven-circle diffractometer (Salje 1995). The detector was a two-dimensional, planar wire detector with either 512×512 or 1024×1024 pixels. All angles were optimized with the ω -angle as the rocking angle and 2θ and χ as detector angles. During the experiments, the distance between the sample and detector was kept at 24 cm. Two pairs of slits controlled the divergence of the incoming beam: while the one closest to the source optimized the beam in the sample, the second slit was fixed at 0.3 mm \times 0.3 mm size. The angular scanning step was 0.06° , with an average counting time per step of three hours. All angles were then transformed into reciprocal-space coordinates (q_x , q_y and q_z) taking as the origin the Bragg position, and displayed with length scales in units of \AA^{-1} (Locherer *et al* 1999). For each sample several reflections were measured, and their patterns visualized as three-dimensional images using an AVS graphics package (AVS 1992). For each of these reflections, the intensity decay along the three main directions of the crystal was then analysed using a subsection of the experimental data set with the appropriate diffraction angles.

3. Results

The three-dimensional equi-intensity surface of reflection (400) of the Moroto sample is shown in figure 1. The centre of the coordinate axes is placed at the maximum intensity of the Bragg peak. In figure 1 the following intensity distributions are shown: (i) the extended Bragg peak,

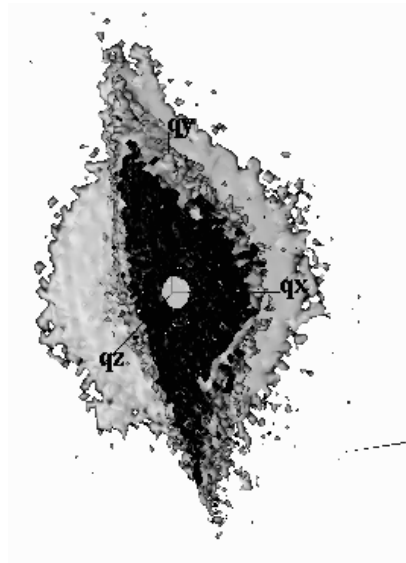


Figure 1. A three-dimensional image of the intensity of reflection (400) for the Moroto sample. The two equi-intensity surfaces indicate the intensity distribution close to the Bragg peak (small surface) and that of the diffuse scattering (large surface). The length of the axes is about 0.015\AA^{-1} .

indicated by the smallest equi-intensity surface (at intensities ten times weaker than that at the maximum of the Bragg peak); and (ii) the diffuse scattering cloud around the Bragg peak, indicated by the largest equi-intensity surface (at intensities 10^5 times less than that at the maximum of the Bragg peak).

On the left-hand side of figure 2, the views along the three main crystallographic axes of this particular reflection show the large anisotropy of the diffuse scattering. The intensity is mainly spread along q_y - and q_z -directions, and less along q_x . The length of the coordinate axes is the same for all graphs in figure 2 and equal to 0.02 \AA^{-1} . The spread in the q_y - and q_z -directions is characteristic for the intrinsic mosaic of the sample and the enhanced twisting

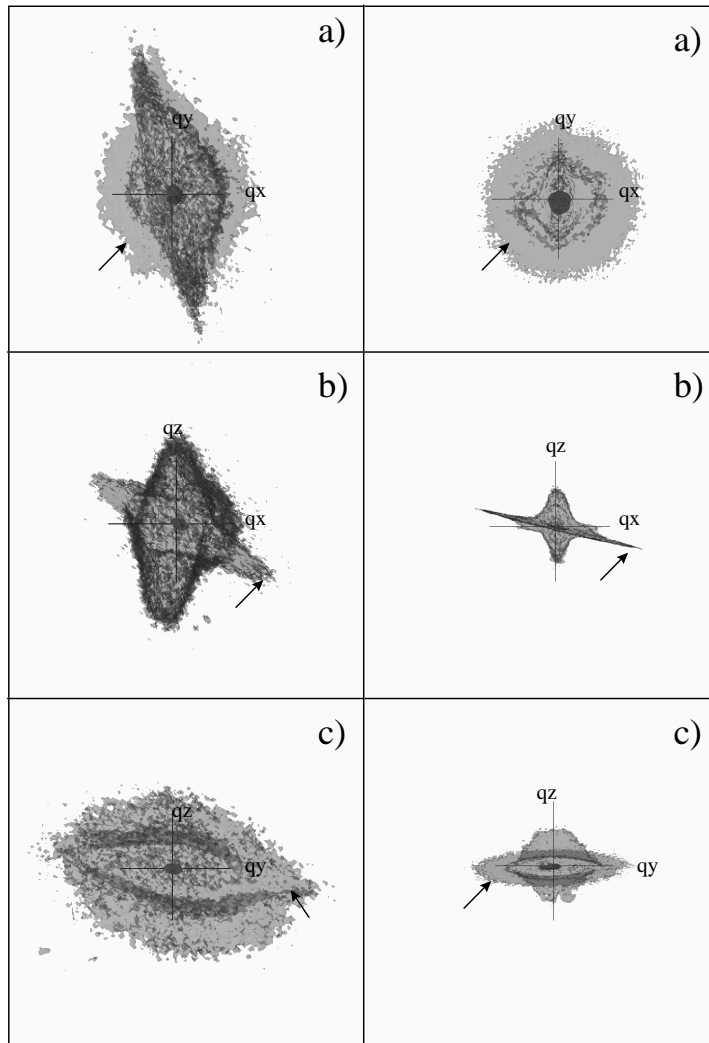


Figure 2. Views along (a) q_z , (b) q_y and (c) q_x for the reflection (400) of the Moroto sample, on the left-hand side, and for reflection (200) of the PHN 4100G sample, on the right-hand side. For comparison, the axis length has been fixed to 0.02 \AA^{-1} in each of the single graphs. The halo present for both samples, and indicated by the arrows, is parasitic scattering due to beam divergence.

of the lattice planes caused by the swelling of the defective areas. The twisting of the lattice planes is larger along the b -axis than along the c -axis, as seen from the elongation of the cloud of diffuse scattering in figure 2(c) for the Moroto sample. The PHN 4100G sample has a very low concentration of radiogenic impurities and can thus be approximated as an 'ideal' zircon sample. The spread of the scattering intensity in reciprocal space is much reduced in this sample; see the right-hand side of figure 2. The diffuse scattering of the PHN 4100G sample shows nearly the same spread of intensity along both directions q_y and q_z .

In radiation-damaged samples the centre of the diffuse cloud does not coincide with the position of the Bragg peak (Holland and Gottfried 1955, Murakami *et al* 1991, Salje *et al* 1999). For the Moroto sample (figure 2) the centre of the diffuse scattering is shifted to larger scattering vectors in the q_x -direction. The resulting asymmetry of the (200) reflection in sample 269 is shown in figure 3. As the measurements were performed on single crystals, the asymmetry observed is directly related to the existence of compressed crystalline areas inside the damaged matrix (Salje *et al* 1999). The swellings of the defective areas and amorphous areas create a differential strain of less than 0.2% between the crystalline damaged matrix and the compressed crystalline islands, as seen in the most damaged sample in our present work, sample 269. Figure 2 shows that for PHN 4100G the centre of the diffuse cloud coincides with that of the Bragg peak. In this case, although compressed/expanded areas do also exist, the differential strain is very small, which makes it difficult to separate the centre of the diffuse scattering from that of the Bragg peak.

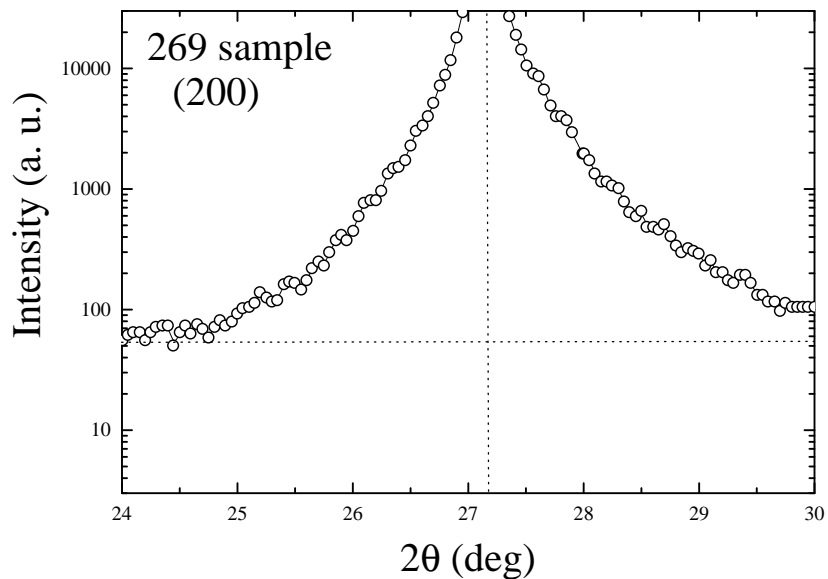


Figure 3. Angular distribution of the x-ray scattering intensity around the (200) reflection for the 269 sample. The asymmetry of the peak is clearly visible.

In order to obtain more quantitative results, the correlation between the diffraction intensities and the scattering vectors was extracted from the data sets collected. Figure 4 shows the intensity distribution along the three main crystallographic axes in a log-log plot for the (200) reflection for all four samples. The (200) reflection is the strongest reflection in zircon and has been systematically measured in all four samples. In order to compare the results from the four different samples, the intensity in figure 4 has been normalized to unity. Note that the

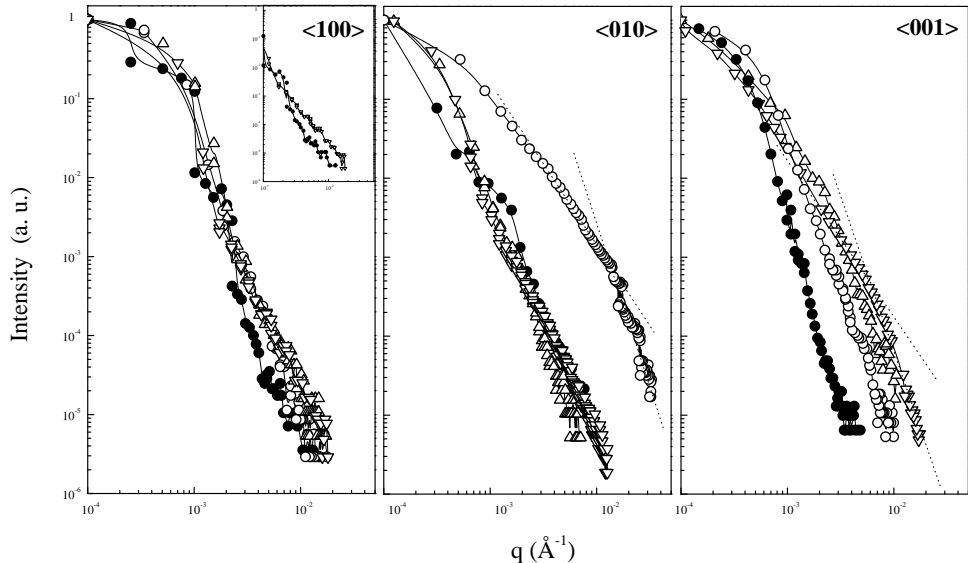


Figure 4. A log–log plot of intensity (normalized to unity) versus wavevector for the (200) reflection along the three main crystallographic axes for each of the four crystals studied: (●) PHN 4100G, (○) 4403, (△) Moroto and (▽) 269. Dotted lines of slope -2 and -4 indicate Huang scattering and Stokes–Wilson scattering respectively.

intensity at the Bragg reflection decreases with increasing radiation damage. For our case, as the degree of damage is rather low, $<2 \times 10^{18} \alpha$ -decay events g^{-1} , the intensity change is by less than a factor of three (Weber (1993) and references therein) and is thus not relevant for our study. The profile in each case may be divided into two parts: the Bragg peak for $q < 10^{-3} \text{ Å}^{-1}$ (which is roughly the halfwidth at half-maximum (HWHM) of the instrumental resolution), and the outer region which behaves differently according to the direction in reciprocal space and the degree of damage.

For the nearly perfect zircon sample, PHN 4100G, no diffuse scattering was observed. The intensity decay in all three directions shows the same behaviour, and is proportional to q^{-4} . This behaviour does not have any physical relevance and should only be associated with the shape of the instrumental function, as observed for a silicon standard crystal. No significant thermal diffuse scattering (TDS) was found. The same intensity decay (q^{-4}) was found for other samples and reflections, like the (440) reflection of sample 4403 (see figure 5), when either there was no diffuse scattering or it was too weak to be observed.

As the degree of damage increases in the crystal, the intensity profiles become more complex. The first feature to notice in figure 4 is that while diffuse intensity appears along the b - and c -axes, hardly any change is observed along the a -axis. The small increase of intensity along the a -axis for high values of q (see the inset of figure 4) is related to the increased shift between the Bragg peak and the diffuse diffraction signal; that is, the peak shape becomes more and more asymmetric. Sample 4403 shows stronger diffuse scattering along the b -axis than the other samples. The intensity of the diffuse scattering relative to the Bragg intensity along the c -axis clearly increases with increasing radiation damage. From all measured reflections it was concluded that the orientation of the diffuse tails was mainly perpendicular to the scattering vector. For reflection (204) in the Moroto sample, for example, no diffuse scattering was found along the $\langle 100 \rangle$ and $\langle 001 \rangle$ directions—figure 6—while strong diffuse scattering occurs in the

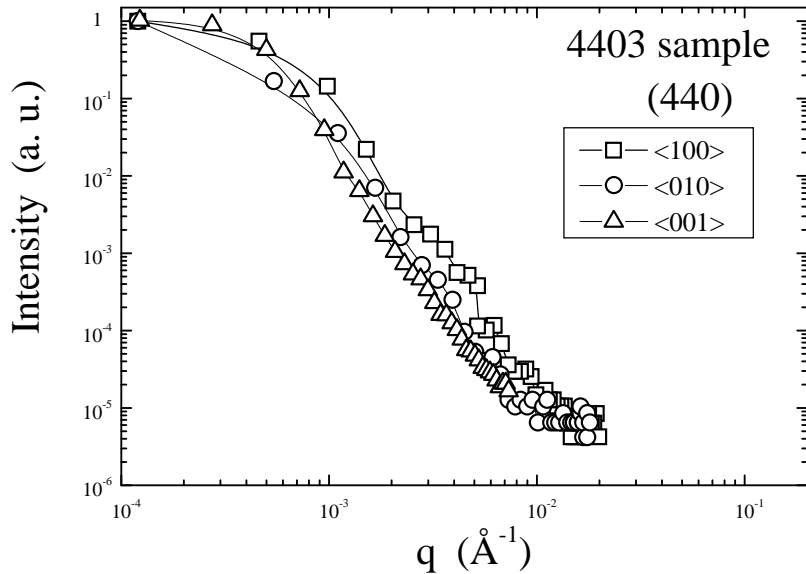


Figure 5. A log–log plot of intensity (normalized to unity) versus wavevector for the (440) reflection in the 4403 sample.

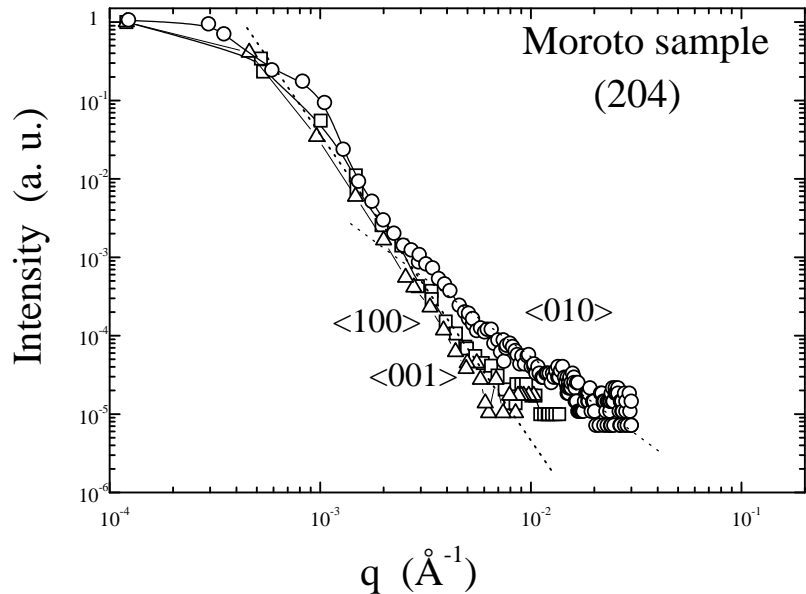


Figure 6. A log–log plot of intensity (normalized to unity) versus wavevector for the (204) reflection in the Moroto sample. In the $\langle 010 \rangle$ (○) direction the Huang scattering can be clearly observed.

$\langle 010 \rangle$ direction. The orientation of the diffuse intensity indicates that the displacement field of the defective areas is mainly transverse with little or no longitudinal contribution.

In agreement with the theory of Huang scattering for point defects and clusters (Huang 1947, Trinkaus 1972, Dederichs 1973), the diffuse intensity observed in zircon close to the

Bragg peak (far away from the point defect or cluster of defects) decays as a function of the wavevector as q^{-2} . This can be seen in figure 4 for sample 4403 along the $\langle 010 \rangle$ direction and for sample 269 along $\langle 001 \rangle$ direction, where this behaviour is indicated by the straight line of slope -2 . A similar result is shown in figure 6. For larger values of the wavevector the diffuse intensity decays more rapidly, as q^{-4} ; this is indicated in figure 4 by the straight line of slope -4 . This type of behaviour is typical for defect clusters where the diffuse scattering (Stokes–Wilson scattering) comes from the strongly distorted region around the cluster. From the crossover between the region where Huang scattering (q^{-2}) dominates and the region where Stokes–Wilson scattering (q^{-4}) dominates, one may obtain a characteristic length scale for the defective area or cluster. The cluster size in sample 4403 was estimated to be about 70 Å. For sample 269, which has a higher degree of radiation damage, we obtain a larger value of ≈ 140 Å. One may expect, for higher doses, the defective areas to start to *touch* each other creating larger defective areas or clusters of larger size.

4. Discussion

In this paper we have reported for the first time on the defect generation by radiation damage in the technologically most important Pu host material (Ewing *et al* 1995), namely zircon. In such studies we have to rely on the investigation of natural minerals (i.e. geological samples) because synthetic materials with sufficiently high defect concentration would be highly radioactive and could not be studied under laboratory conditions. Geological samples, on the other hand, have accumulated high defect concentrations over geological times that are longer than the lifetime of the relevant radiogenic impurities.

We observe several features which appear counterintuitive at first glance. Firstly, we find that the Bragg reflections are rather sharp with little longitudinal diffuse scattering, indicating that the lattice parameters a and c do not vary much within the diffracting volume. This observation is important as it demonstrates that the radiation-induced swelling of the unit cell occurs much more uniformly (in chemically uniform samples) than previously thought (Murakami *et al* 1991). If the swelling of the unit cell is due to localized defects (interstitials, Frenkel defects etc), then we conclude that these defects are rather uniformly distributed in the sample. It is not clear yet whether such uniform defect distributions are the result of the initial defect creation through the scattering of α -particles or due to the equilibrium of the defects after the α -decay event. In the former scenario the defects are scattered during the creation process, while in the second scenario the defects need to have sufficient mobility for their rearrangement.

In contrast to the high spatial uniformity of the longitudinal unit-cell swelling, our second main result indicates that large non-uniform structural variations exist as transverse shear waves. These shear waves are the origin of the strong diffuse Huang scattering which characterizes the radiation-damaged state in zircon. These transverse deformation waves have not been observed in previous work. Diffuse streaks were observed by electron diffraction measurements (Meldrum *et al* 1998) for samples in the stage prior to complete amorphization. However, at this stage the diffuse streaks are due to the relative misorientation of the few crystalline areas still surviving in the amorphous matrix.

As pointed out in the previous section, the Huang scattering was observed to be larger in the basal plane than along the c -axis. This result is directly correlated with the crystal structure of zircon. Zircon is characterized by edge-sharing ZrO_8 polyhedra in the basal plane connected along the c -axis by edge-sharing SiO_4 tetrahedra (Speer 1982). Our results show that the lattice planes are more twisted in the ab -plane than along the tetragonal direction, which may well indicate that the structure relaxes more easily in this plane than along the

c-direction, where the atomic bonds are stronger. This is in agreement with previous work (Holland and Gottfried 1955) which showed that the swelling of the unit cell in the *ab*-plane is lower, for low radiation doses (the case of our study), than along the *c*-axis. Moreover, the elastic constant in the *ab*-plane ($C_{11} = 4.229 \times 10^{12}$ dyn cm $^{-2}$) is slightly smaller than that along the *c*-axis ($C_{33} = 4.903 \times 10^{12}$ dyn cm $^{-2}$) (values for synthetic zircon, from Özkan *et al* 1974) which also explains why the structure is easier to deform in the *ab*-plane than along the tetragonal axis.

We now focus on the open question of the origin of this shear deformation in radiation-damaged zircon. Two possible scenarios can be envisaged. Firstly, the cascade of displaced atoms generated by the α -particles is thought to occur on a timescale of a few picoseconds (Díaz de la Rubia 1996). This cascade will generate strain fields in the crystalline lattice which will propagate roughly with the velocity of sound. After the initial expansion the cascades will rapidly anneal, although several defects are expected to remain in the structure. These defects may well then stabilize the deformation waves in a geometrical arrangement which may represent a local energy minimum. The shear waves are then localized around defect clusters of some 70 Å in diameter. The origin of the shear waves is in this case related to the local defects in the crystalline part of the sample. Alternatively, one might also think that the observed shear deformation is generated by the strain fields created in the surrounding areas of the amorphous islands. In this case the shear waves are expected to have their largest amplitudes inside the rim of the amorphous islands. The strong diffuse scattering seen in our measurements suggests however that the origin of the shear deformation is distributed more uniformly over the crystalline lattice rather than being due to a relatively small part of the sample. Moreover, if the strain field was due to the swelling of amorphous areas (some 18%, according to Holland and Gottfried 1955), then one would expect to see the shrinking of the lattice parameters in the same part of the sample, i.e. diffuse scattering mainly distributed along the longitudinal direction. Furthermore, the macroscopic swelling in zircon is almost identical to the unit-cell swelling at low radiation doses (Weber *et al* 1994). While in Cm-doped $\text{Ca}_2\text{Nd}_8(\text{SiO}_4)_2$ orthosilicate, where the rate of amorphization is higher than in zircon (Weber 1993), the macroscopic swelling is double the unit-cell swelling. This observation indicates that the structural deformation generated by the rims of the amorphous islands is very limited in zircon, and that the origin of the shear waves is expected to be mostly related to defects in the crystalline parts of the materials.

In conclusion, radiation-induced localized defects in zircon generate transverse shear waves, the uniform lattice expansion being only a secondary effect. The shear waves have not been seen previously, although they appear to dominate the microstructure of radiation-damaged zircon.

Acknowledgments

The authors are very grateful to the National History Museum of London for allowing us to use zircon samples from their collection, in particular 269 (BM.1920, 269) and PHN 4100G (BM.1998, P2(3366)G). The authors also wish to thank Dr H Chapman (Department of Earth Sciences, University of Cambridge, UK) and Professor R Parrish and Dr G Nowell (Department of Geology, Leicester University, UK) for providing us with the sample PHN 4100G, and Professor R C Ewing (Department of Nuclear Engineering and Radiological Sciences, University of Michigan, USA) for letting us use sample 4403. We also thank Dr S Reed (Department of Earth Sciences, University of Cambridge, UK) for his help in the electron microprobe analysis. This research project was supported by the European TMR Network contract number FMRX-CT97-0108 (DG12-SLJE).

References

AVS 1992 *Application Visualization System. Developer's Guide and Applications Guide* Advanced Visual Systems, Incorporated, Waltham, MA, USA

Chakoumakos B C, Murakami T, Lumpkin G R and Ewing R C 1987 *Science* **236** 1556

Dederichs P H 1973 *J. Phys. F: Met. Phys.* **3** 471

Díaz de la Rubia T 1996 *Annu. Rev. Mater. Sci.* **26** 613

Ewing R C, Chakoumakos B C, Lumpkin G R and Murakami T 1987 *Bull. Mater. Res. Soc.* **15** 58

Ewing R C, Lutze W and Weber W J 1995 *J. Mater. Res.* **10** 243

Holland H D and Gottfried D 1955 *Acta Crystallogr.* **8** 291

Huang K 1947 *Proc. R. Soc. A* **190** 102

Locherer K R, Buckley A and Salje E K H 1999 *J. Appl. Crystallogr.* **32** 362

Meldrum A, Boatner L A, Weber W J and Ewing R C 1998 *Geochim. Cosmochim. Acta* **62** 2509

Murakami T, Chakoumakos B C, Ewing R C, Lumpkin G R and Weber W J 1991 *Am. Mineral.* **76** 1510

Nowell G 1999 private communication

Özkan H, Cartz L and Jamieson J C 1974 *J. Appl. Phys.* **45** 556

Salje E K H 1995 *Phase Transitions* **55** 37

Salje E K H, Chrosch J and Ewing R C 1999 *Am. Mineral.* **84** 7

Speer J A 1982 *Orthosilicates (Reviews in Mineralogy vol 5)* ed P H Ribbe (Washington, DC: Mineralogical Society of America)

Trinkaus H 1972 *Phys. Status Solidi b* **51** 307

Weber W J 1981 *J. Nucl. Mater.* **98** 206

Weber W J 1993 *J. Am. Ceram. Soc.* **76** 1729

Weber W J, Ewing R C and Wang L M 1994 *J. Mater. Res.* **9** 688